(Received 23 July 2025, Accepted 17 August 2025, Scheduled 24 August 2025)

1-Bit Reconfigurable Reflectarray for Short-Range Wireless Systems

Juwanto, Said Attamimi, Umaisaroh, and Mudrik Alaydrus*

Department of Electrical Engineering, Universitas Mercu Buana, Jakarta, Indonesia

ABSTRACT: This paper presents the design, simulation, and experimental validation of a 1-bit reconfigurable reflectarray. Each unit cell is equipped with a single PIN diode, enabling binary phase control (0° and 180°) for dynamic beam steering. The reflectarray employs a compact and cost-effective architecture, with digitally reconfigurable elements that allow real-time control of the reflected wavefront. The integration of PIN diodes ensures fast switching and low power consumption while maintaining good reflection efficiency and phase performance. Without limiting the applicability of the method, a reflectarray antenna consisting of 9×9 element array operating at 5.8 GHz was designed. Full-wave electromagnetic simulations and measurements demonstrate beam steering capability up to $\pm 15°$, with minimal gain degradation and acceptable side-lobe levels. The proposed reflectarray design is a promising solution for low-complexity, reconfigurable antenna systems in applications such as wireless communications, radar, and IoT systems operating in the 5.8 GHz ISM band.

1. INTRODUCTION

The ability for beamsteering of an antenna is essential to improving the signal quality in a wireless system [1]. Transmitarray and reflectarray antennas are high-gain antennas that exploit the advantages of planar array structures and simple beam optics techniques. In the past, various unit cell structures with different geometrical shapes and dimensions have been developed to meet these objectives [2]. Depending on the shape and geometry of the designed unit cell, beamsteering can be obtained in the azimuth and/or elevation direction according to the desired direction.

In [3], an analytical study was conducted on the effect of the number of layers to the phase range. The results showed that the more the layers are used, the wider the phase range is obtained. Abdelrahman et al. in [4] gave the result of 360° phase range with a four-layer structure with a total thickness of 0.75λ. The transmitter array consists of a cross slot in a metal sheet as the unit cell element. A two-layer transmitter array with a Maltese cross is proposed in [5]. The Maltese cross structure is connected through four holes; this antenna achieves a gain of 33 dBi and an aperture efficiency of 40%. Pham et al. [6] proposed a metal-specific C-shaped unit cell for applications at 29.5 GHz. The transmitter array consists of three layers with a total thickness of 0.59λ, a gain of 29.9 dBi, and an aperture efficiency of 50.9%.

Previously, a transmitter antenna has been suggested in [7]. The antenna consists of three layers operating at X-band frequency with 537 spiral dipole elements. The gain of the transmitting antenna is 28.9 dBi at 11.3 GHz. In [8], a triple-layer transmitarray antenna has been implemented. The shape of the unit cell patch is a split diagonal cross element with 9×9 elements. This antenna operates at 12.5 GHz and has a measured gain of 18.9 dBi. In [9], a triple-layer dual-mode meta-atom with an H-shaped structure at X-band frequency has been implemented. The quad-beam transmitarray consists of 25×25 elements and has a peak gain of 18.8 dBi at 9.6 GHz. Another triple-layer transmitarray antenna is presented in [10]. The unit cell combines a cross-slot configuration and a double square ring. The antenna gain at 12.4 GHz is 25.8 dBi. The transmitarray consists of 233-unit cell elements etched in a circular shape with a diameter of 221 mm and a total thickness of 15 mm (0.62λ). Recently, Dewi et al. [11] presented a double-layer transmitarray antenna with a 4 mm aperture with a unit cell element consisting of two open rectangular resonator loops. The antenna operates at a frequency of 9.8 GHz; it has a maximum calculated gain of 18.4 dBi, a maximum measured gain of 18.5 dBi, and an aperture efficiency of 31.7%. Unlike ordinary reflector antennas, the flat surface of the reflectarray antenna and the nature of the microstrip involved in it limit the working bandwidth of this system. Both produce phase errors, which have implications for disturbed transmission patterns or reduced gain [12, 13]. Several methods have been proposed to improve this condition, such as modifying the shape of the aperture [14] or using additional elements that produce additional delays of the wave components [15]. To increase the working bandwidth of this antenna, several methods have been proposed, such as multilayered configurations, involving layers whose elements resonate at different frequencies [16–19], phase-shifting elements arranged in a network smaller than the wavelength [20], the use of thick substrates [21], and proper optimization of the phase distribution in the antenna plane structure. The last technique is important because in a reflectarray configuration, the phase difference between elements is responsible for producing a specific radiation pattern, and the phase response requirements of each element do not fully guarantee the overall antenna behavior at other frequencies [22, 23].

* Corresponding author: Mudrik Alaydrus (mudrikalaydrus@mercubuana.ac.id).

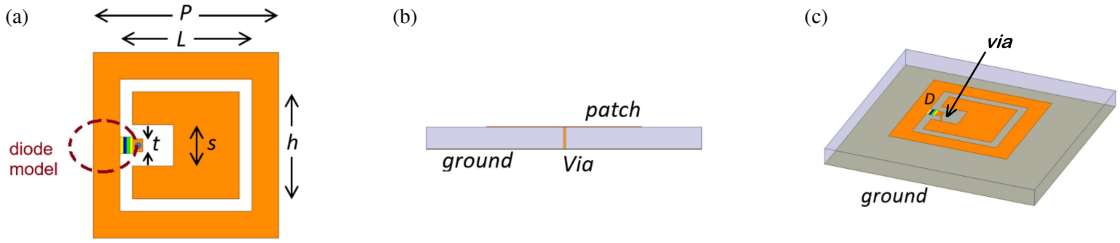

FIGURE 1. Unit Cell, (a) detailed geometry of the patch, (b) side view of connecting via, (c) perspective view.

Several other methods used to design reflectarray antennas with linear polarization that have large bandwidths are given in the form of single-layer elements with additional transmission lines to change the phase [24, 25], elements smaller than the wavelength but with large phase shift capabilities, or four-arm spiral elements with varying lengths [26]. In recent years, various researches have also been conducted on reflectarray antennas at millimeter frequencies (28 GHz and 38 GHz) which are strong candidates for 5G and 6G systems [27–31]. Adaptive transmission and reflection capabilities in the form of intelligent reflecting surfaces (IRSs) are believed to play an important role in 6G wireless communication networks [32, 33].

Other analytical approaches for radiation synthesizing were presented in [34]. Antenna arrays are partitioned using T-shaped tetromino subarrays to reduce cost and complexity. Two architectures are optimized with a genetic algorithm, achieving sidelobe levels below -20 dB and -25 dB, while simplifying the feeding network. Ref. [35] presents a simple method for reconfiguring antenna beam-patterns using a thinned element approach. By dividing array elements into three groups with fixed, adaptive, and zero weights, and optimizing the middle group via a genetic algorithm, the method enables easy switching between narrow and wide beams while controlling sidelobes and nulls. In [36], a pixel-based method enables low-cost beam reconfiguration by turning array elements ON or OFF, without phase shifters. It supports various shapes, with reduced gain but verified effectiveness via some computer simulations.

Most of the existing studies on IRS and its applications for wireless communication are only about theoretical analysis with simulation as validation. Therefore, an important research direction is to confirm theoretical results with data from real-world system implementations and experiments. The basis of using diode switches is developed for signal steering to the main angles of $0°$, $-40°$, and $+40°$ [37]. This model can more accurately guide the optimization of IRS for more transmitting directions to help wireless communication.

In this paper, we follow the reconfigurability of a reflectarray antenna by using a number of PIN diodes in 9×9 unit cell elements. The antenna works at 5.8 GHz. Each PIN diode can be biased independently from each other, so that with these 9×9 elements, theoretically there are 2^{81} switching combinations available.

2. DESIGN OF RECONFIGURABLE REFLECTARRAY

The design of the complete reflectarray begins with a proposed unit cell as described in Subsection 2.1. The unit cell is etched on a Rogers 5880 substrate ($\varepsilon_r = 2.0$, $\tan\delta = 0.0009$) with a thickness of 1.57 mm backed by ground. In Subsection 2.2, the modeling of PIN diodes for forward and reverse biased conditions is presented suitable for numerical calculation in software ANSYS High Frequency Structure Simulator (HFSS). Subsection 2.3 is dedicated to the detailed observation of reconfigurable unit cell and its consequences for designing 1-bit reconfigurable reflectarray antennas. After some parameter studies, based on the unit cell, a complete reconfigurable reflectarray fed by an aperture horn antenna is proposed in Section 3.

2.1. Unit Cell

Using ANSYS HFSS program, a design of the unit cell was proposed as a basic structure to build the reflectarray antenna. The unit cell is embedded in a region surrounded by a periodic boundary condition and a Floquet port for excitation. This setting enables a periodic continuation of the unit cell in a two-dimension extension. In the simulation, some geometrical parameters are proposed and optimized, so that certain desired reflection coefficient (S_{11}) values can be achieved.

Figure 1 gives the detailed structure of the geometry of the proposed unit cell. The unit cell consists of the front side, the so-called patch as given in Fig. 1(a), which is connected to the ground via a conducting pin with a radius of 0.1 mm as depicted in Fig. 1(b). A perspective view of the proposed unit cell is shown in Fig. 1(c).

The dimension of the unit cell depends primarily on the side length of the rectangular resonator,

$$P = \frac{c}{4f\sqrt{\varepsilon_{r,eff}}} \tag{1}$$

which becomes around 10.5 mm at the frequency of 5.8 GHz and with the effective relative permittivity of the substrate of $\varepsilon_{r,eff} = 1.5$. Other geometrical parameters are given in Table 1.

With this information, it is expected that the magnitude of the reflection coefficient is as close to 0 dB as possible. In or-

TABLE 1. Geometry of the proposed unit cell.

Parameter	P	L	h	s	t
Value [mm]	10.5 . . . 12	8	6.5	2.5	0.5

FIGURE 2. Equivalent circuit model for PIN diode, (a) forward bias (on state), (b) reversed bias (off state).

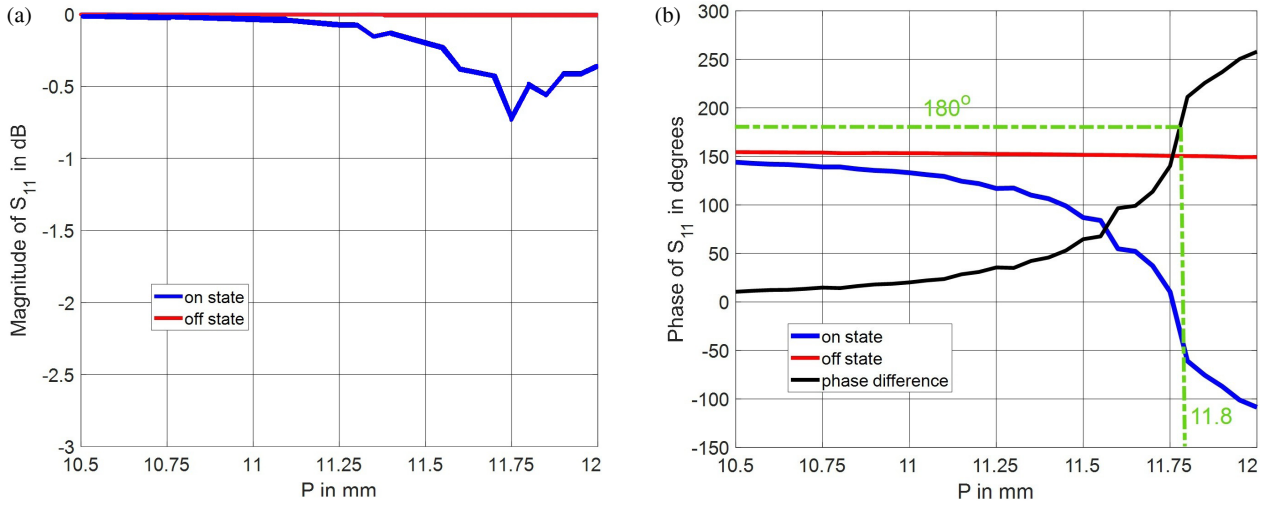

FIGURE 3. Reflection coefficient of the unit cell for on/off state of the PIN diode at 5.8 GHz as function of parameter P, (a) magnitude of the reflection coefficient, (b) phase of the reflection coefficient and its phase difference.

der to make a large phase variation, the dimension of the unit cell P was varied between 10.5 and 12 mm by considering the grounding effect of the rectangular resonator. To realize this circumstance, a direct connection from the patch to the via hole was built, or to break the connection between them. These conditions will be implemented using PIN diodes, which will be explained in Subsection 2.2.

2.2. Modeling the PIN Diode

In order to reconfigure the unit cell, as visualized in Fig. 1, a PIN diode is connected between the closed rectangular loop and the via. In the conducting case (on state), the electric current would flow from the loop to the ground, whereas a reversed bias (off state) would prevent it. In this work, BAR64-02W from Infineon Technologies was used. Dependent on the bias, the diode behaves differently, so that two different equivalent circuit models are available to describe their physical characteristics. Two equivalent circuits, as sketched in Fig. 2, are adopted to model the diode in on and off states. For the forward bias, the values $R_s = 3$ ohms, $L_s = 0.6$ nH were proposed, whereby for the reversed bias, $R_p = 5$ kohms, $C_T = 0.15$ pF, and $L_p = 0.6$ nH. These values lead to the magnitudes of impedance around 20 Ω and 179 Ω in on and off states, respectively.

The circuit model is implemented for both on and off states in the form of lumped elements. In this way, the off state model is expected almost no phase variation in the reflection coefficient, whereas in the on state, due to direct connection between the resonator and ground, it is expected to obtain a large phase variation of the reflection coefficient.

2.3. Simulation of the Reconfigurable Unit Cell

The unit cell with integrated lumped elements for modeling the on and off states was simulated at 5.8 GHz, and the reflection coefficient was calculated as given in Fig. 3 as a function of the side length of the resonator P. The magnitude of the reflection coefficient for on state, as indicated by blue curve, is very close to 0 dB across the P range (from 10.5 mm to 12 mm). It means that the unit cell reflects nearly all incident power in the on state, which represents a high reflection efficiency. This is a good characteristic for a reflectarray unit cell. On the other hand, the magnitude of the reflection coefficient for off state (red curve) shows a variation with P. As P increases, $|S_{11}|$ drops to -0.8 dB at $P \approx 11.65$ mm but never below -1 dB, which is still acceptable. However, the magnitude of the reflection coefficient is lower than that in the on state, implying some loss or absorption in the off state — possibly due to higher resistive components or surface wave excitation.

The phase characteristic (as given in Fig. 3(b)) for on state (blue curve) decreases gradually and nonlinearly with increasing P. It covers a range from about $145°$ to $-130°$, which indicates a strong tunability. This tunable range is very useful for dynamic beamforming. On the other hand, for off state (red curve), the phase is almost constant (around $150°$) across all values of P. It suggests that in the off state, the unit cell is not responsive to P variation, behaving like a fixed passive surface.

Moreover, Fig. 3(b) shows the phase difference (black curve) representing the difference between on and off states,

$$\Delta\varphi(P) = \angle S_{11,off}(P) - \angle S_{11,on}(P) \quad (2)$$

At $P \approx 11.8$ mm, the phase difference hits around 180°, which is ideal for binary phase modulation (i.e., 0° and 180° states). This point is marked with green dashed lines and highlights an optimal switching condition. The proposed unit cell design demonstrates excellent performance for 1-bit reconfigurable reflectarrays at 5.8 GHz. For next observation, the value $P = 11.8$ mm is used for the design. A further investigation of this unit cell shows that the condition for binary phase modulation is effective in the frequency interval of 5.74 GHz to 5.89 GHz.

3. RESULTS AND DISCUSSION

In this section, a reflectarray consisting of 9×9 patches is built. In each patch, a PIN diode is attached to allow a direct connection to the ground. All diodes can be switched on or off independently from each other, so that theoretically there are 2^{81} possible connection combinations. The overall dimension of the reflectarray is 125 mm × 125 mm × 1.57 mm. An aperture antenna WR137 (dimension 34.85 mm × 15.80 mm) was used as a feed for the reflectarray. As illustrated in Fig. 4, the feed antenna is mounted symmetrically in the middle position with a focus distance of 34.4 mm. This value was chosen to optimize the balance between illumination loss and spill over loss.

After getting the complete geometrical and electrical data from Section 2 and additional information given in Fig. 4, the model is covered by a radiation boundary condition to guarantee that there is only radiation from the reflectarray. We continue with the following observations and set some of the diodes on and the other off as given in Fig. 5. In computer simulation, the on state is represented by setting the equivalent circuit as given in Fig. 2(a), whereas the off state is modeled by the representative equivalent circuit in Fig. 2(b). For better overview, the on state is visualized by blue color and the off state by orange color. The results of computer simulation will be compared with measurements later at the end of this section.

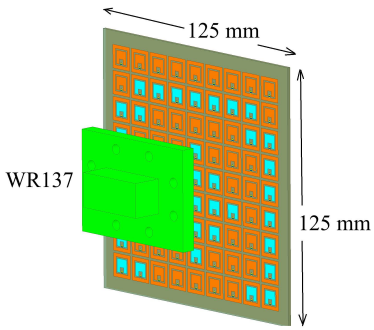

FIGURE 4. Perspective view of the computer model for designed reflectarray with a feed antenna WR137.

Figure 6 gives the normalized radiation patterns of a reconfigurable reflectarray antenna operating under three different control states: Setting 1 (solid red line), Setting 2 (dash-dot black line), and Setting 3 (dashed blue line). The radial axis represents normalized gain in linear scale from 0 to 1, while the angular axis represents azimuthal angle φ in degrees. These radiation patterns demonstrate how the antenna beam can be actively controlled by switching among different phase configurations, with each setting producing a distinct main lobe direction and pattern shape. In Setting 1, the antenna radiates predominantly toward $\varphi = 0°$, and two side lobes in directions $\varphi = 90°$ and $\varphi = 270°$. Setting 2 results in a slightly narrower beam directed to around $\varphi = 345°$, with a reduction in the forward lobe compared to Setting 1, and the side lobes remain in directions $\varphi = 90°$ and $\varphi = 270°$ with reduced intensity. In Setting 3, the main lobe shifts to reverse direction compared to Setting 2, and it is pointed to around $\varphi = 15°$, whereas the side lobes are the same as in Setting 2. This progressive beam redirection confirms that the antenna system achieves dynamic beam steering through reconfiguration, which is crucial for applications such as adaptive radar, wireless power transfer, or beamforming in mmWave communications.

From a performance standpoint, each configuration exhibits unique radiation characteristics, highlighting trade-offs inherent in low-bit reconfigurable designs. Setting 1 offers the highest normalized peak gain (1.0), implying optimal phasing and constructive interference in that state. However, it also exhibits pronounced sidelobes, especially in the backward direction ($\varphi \approx 180°$), which can lead to unwanted radiation and reduced efficiency. Setting 2, while maintaining a similar beam directionality, shows a slightly lower peak gain (0.7) but reduced backlobes, suggesting improved suppression of backward scattering. Setting 3 demonstrates the lowest forward gain (0.6) and a broader main lobe, indicating more diffuse radiation likely due to less optimal phasing or broader coverage requirements. All three settings display some sidelobe and backlobe structures, typical in systems employing 1-bit or coarse phase quantization, where each element can only shift the phase between two values (e.g., 0° and 180°). This quantization limits beamforming precision and increases spectral leakage. Nonetheless, the demonstrated control over the main beam direction—even with moderate peak variation—validates the design's effectiveness as a directionally reconfigurable antenna. Future improvements could focus on increasing phase resolution (e.g., to 2-bit or 3-bit levels), integrating amplitude tapering to suppress sidelobes, or optimizing the array's surface geometry. Overall, the plot successfully confirms the functionality of the antenna's dynamic reconfigurability, while also providing a clear basis for analyzing and improving directional gain, beamwidth, and sidelobe behavior across operational modes.

In order to verify the simulated radiation pattern, the complete reconfigurable reflectarray was fabricated. To make a passive reflectarray antenna into an active reflectarray is to add a circuit as a controller when the PIN diode is on and off. As previously discussed to turn on the diode, a certain direct current (DC) voltage must be applied with forward bias on the diode. The applied voltage value ranges from 0.6 volts to 0.8 volts. In this study, a switch circuit was implemented as a controller or provider of DC voltage from the battery to the diode. To prevent the alternating current (AC) voltage to enter the DC controller, an inductor (L) needs to be installed on the DC path. The inductor component acts to block AC voltage but passes

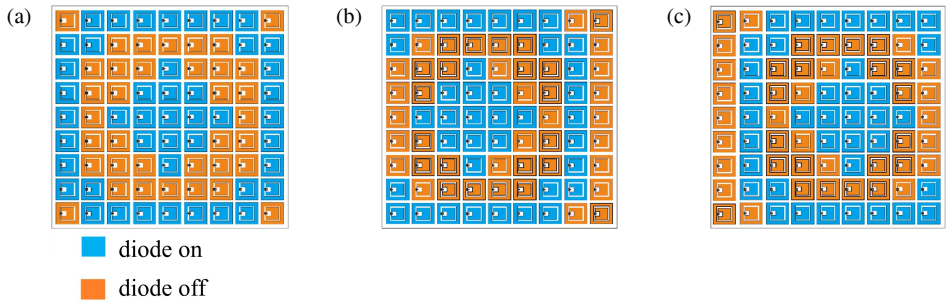

FIGURE 5. On-off setting combinations, (a) setting 1, (b) setting 2, (c) setting 3.

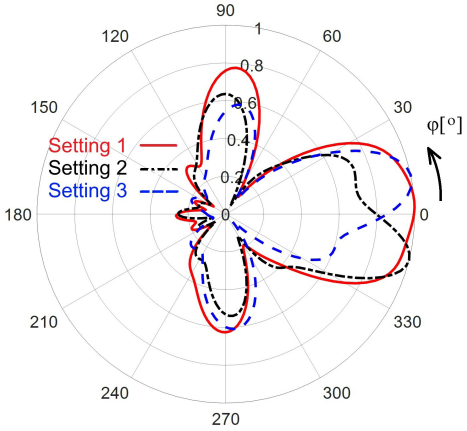

FIGURE 6. Simulated radiation diagram in horizontal plane.

DC voltage. Moreover, to prevent excessive DC voltage on the PIN diode, a resistor component needs to be installed in series with the inductor. This resistor acts to withstand excess current passing through the PIN diode. In this work, 0603 SMD/SMT 1% Resistors with the value of 1 kOhm and 1206 SMD SMT Chip Inductors with the value of 22 µH were used. They have an impedance value of around 800 kOhm at the frequency of 5.8 GHz, which represents an 'open' circuit for the RF signal.

Another important thing in designing a controller is how the DC path does not interfere with the patch performance. Because the position of the controller is far from the reflectarray, there will be a cable path from the controller to the diode pin on the antenna patch. This reflectarray antenna design has a total of 81 patches, meaning that the number of diode pins and DC lines is also a minimum of 81, plus one ground line. In order not to interfere with the antenna patch, the DC line was placed on a printed circuit board (PCB) that is separate from the antenna PCB. In Fig. 7, there are two PCBs. Fig. 7(a) shows PCB 1 as the place where the antenna patches are printed, and Fig. 7(b) gives PCB 2 for DC supply. PCB 2 is located behind the antenna PCB. Between PCB 1 and PCB 2 there is a ground layer to block the electromagnetic fields. For the sake of miniaturization, surface mounted device (SMD) diodes, inductors, and resistors were used.

After all antenna components are assembled, the reflectarray antenna is located on a rotating table 1.0 m apart from RS HF907 as measuring antenna, as given in Fig. 8(a). The antennas were connected to RS ZVA67 Vector Network Analyzer (VNA), and the measurement was carried out in Microwave Laboratory Universitas Mercu Buana, Jakarta. For comparison purposes to the simulation results, here the same three settings were done as indicated by color LEDs in Fig. 8(b).

Figure 9(a) shows the comparison between the calculated (red solid line) and measured (blue dashed line) radiation patterns in the horizontal plane for Setting 1. Both patterns are normalized, with amplitude values ranging from 0 to 1. The comparison reveals good agreement in terms of main lobe direction, with both the simulation and measurement showing strong radiation toward $\varphi \approx 0°$. However, some discrepancies are evident: the measured pattern shows more irregular sidelobes and ripples, particularly between $\varphi = 180°$–$300°$, likely due to fabrication imperfections, measurement noise, or environmental reflections. The calculated pattern is smoother and exhibits idealized symmetry, which is typical of simulation results that assume perfect material properties and boundary conditions. Overall, the plot demonstrates that the antenna performs as designed, with acceptable alignment between theory and experiment, though refinements may improve the match further.

Figure 9(b) presents a comparison between the simulated (red solid line) and measured (blue dashed line) radiation patterns of a reconfigurable reflectarray antenna in the φ-plane for Setting 2. The simulation predicts a strong main lobe around $\varphi \approx 345°$, which is generally confirmed by the measured pattern, though with some angular shift and reduced amplitude, especially in the 60°–120° region. Notably, the measured pattern shows more distortion and sidelobe fluctuation, likely caused by environmental reflections, manufacturing tolerances, or array element mismatch. Despite these deviations, the overall beam directionality and shape are in reasonable agreement, confirming the antenna's beam-steering functionality. The differences between the calculated and experimental data highlight practical limitations often encountered during prototype testing but also indicate that the design model is fundamentally sound, offering a good foundation for further refinement.

Figure 9(c) displays the comparison between simulated (red solid line) and measured (blue dashed line) radiation patterns of a reconfigurable reflectarray antenna for Setting 3. The patterns are normalized, indicating relative radiation intensity across the azimuthal angle φ. The main beam direction in both curves aligns around $\varphi \approx 15°$, suggesting consistent beam steering

FIGURE 7. Fabricated reflectarray, (a) the structure of the patch side with 81 PIN diodes, (b) connection lines for DC supply with 81 SMD resistors and SMD inductors, (c) complete reflectarray system.

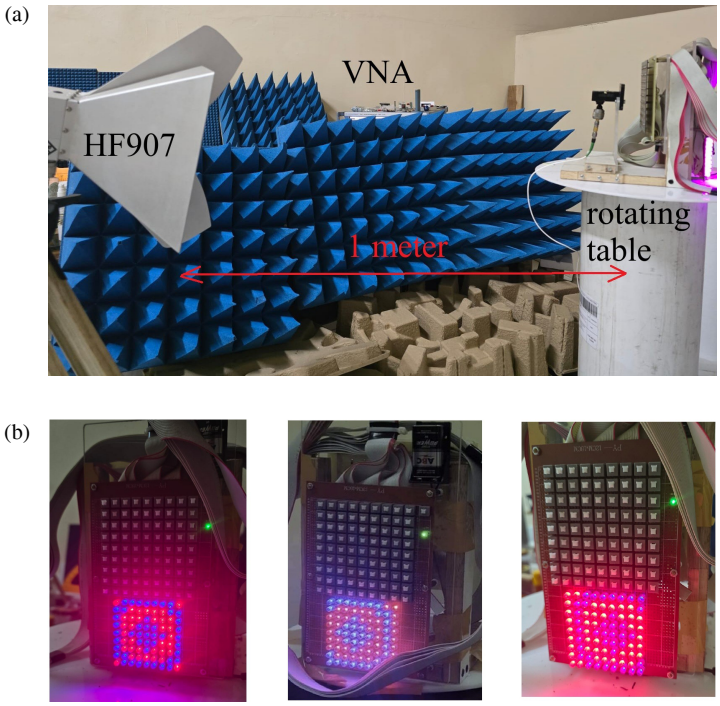

FIGURE 8. Measuring the radiation diagram, (a) testbed, (b) reflectarray with setting 1, 2 and 3.

between simulation and measurement. The measured pattern, however, exhibits more irregularities, particularly in sidelobes and backlobe region ($\varphi \approx 180°$–$300°$), which may result from measurement noise, fabrication tolerances, or finite array effects not captured in simulation. Despite these discrepancies, the general shape and beam direction are well preserved, indicating a successful realization of the antenna's design objectives. The red (calculated) pattern shows a smoother and more idealized lobe structure, while the blue (measured) pattern reflects practical deviations common in experimental setups. Overall, the agreement confirms the antenna's directional behavior and validates the theoretical model.

Figure 10 shows the gain versus frequency plot of calculated and measured results between 5 GHz and 7 GHz. The red curve represents the calculated gain, which remains relatively flat at around 10.5 to 11 dB across the entire frequency range. In contrast, the blue curve shows the measured gain, which varies more significantly but peaks at approximately 11.1 dB near 5.8 GHz. The measured bandwidth, defined between 5.435 GHz and 6.5 GHz, is 1.065 GHz. Within this range, the gain remains relatively high, mostly above 9.5 dB, indicating effective performance across a wide frequency band. There is a good agreement between the simulated and measured gain values in the central portion of the frequency range, particularly near the peak. However, some discrepancies are observed at the lower and upper ends of the band, where the measured gain drops below the simulated values. These differences are common and can be attributed to real-world factors such as fabrication tolerances, material losses, and measurement uncertainties. Overall, the results confirm that the design performs well, offering a broad operational bandwidth with consistently high gain. The close match between simulation and measure-

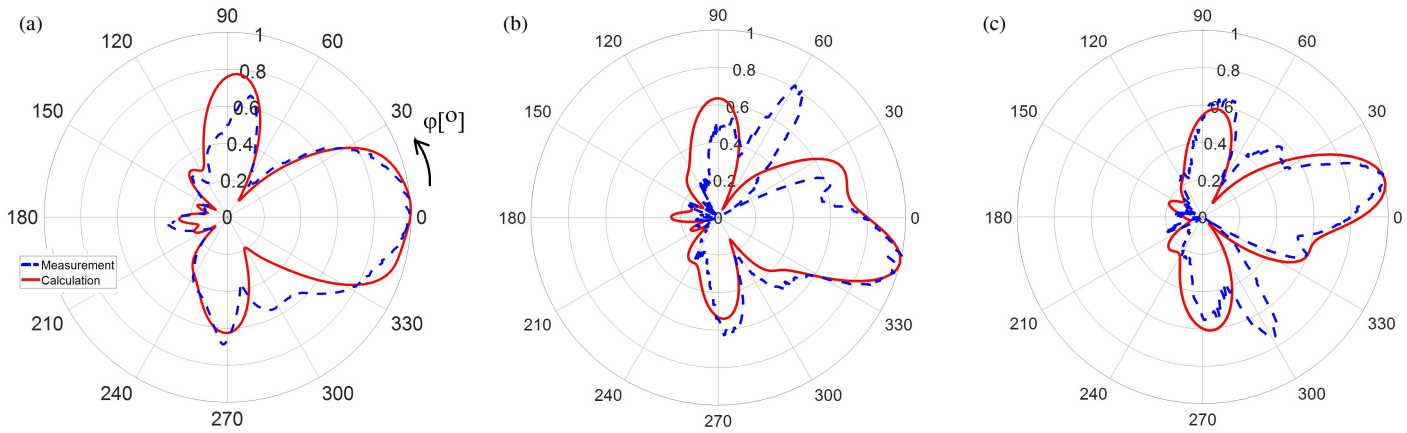

FIGURE 9. Horizontal radiation diagram, (a) setting 1, (b) setting 2, (c) setting 3.

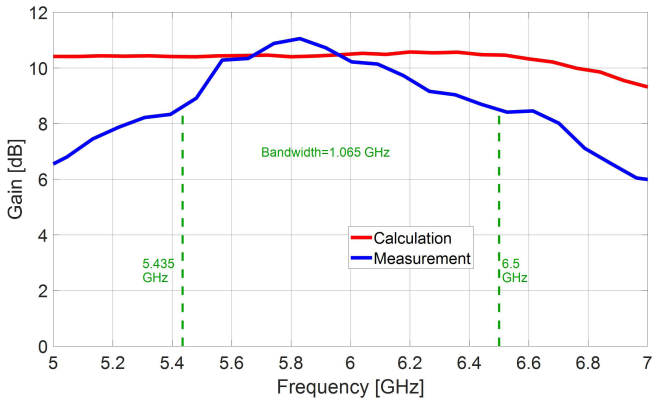

FIGURE 10. Calculated and measured gains as function of frequency.

ment also reflects the reliability and accuracy of the design process.

4. CONCLUSION

A 1-bit reconfigurable reflectarray antenna operating at 5.8 GHz has been successfully designed, simulated, and fabricated. The use of PIN diodes allows binary phase control of each unit cell, enabling effective beam steering through three distinct radiation configurations. Both simulation and measurement results confirm the reflectarray's ability to redirect its main lobe dynamically, demonstrating its suitability for adaptive wireless applications. Future work will focus on enhancing phase resolution, improving sidelobe suppression, and developing control algorithms for real-time beam optimization.

ACKNOWLEDGEMENT

This document is the results of the fundamental research project funded by Kemdikbudristek under contract number 0459/E5/PG.02.00/2024 and 105/E5/PG.02.00.PL/2024; 808/LL3/AL.04/2024; 01-1-4/654/SPK/VII/2024.

REFERENCES

[1] Xu, R. and Z. N. Chen, "A hemispherical wide-angle beamsteering near-surface focal-plane metamaterial luneburg lens antenna using transformation-optics," *IEEE Transactions on Antennas and Propagation*, Vol. 70, No. 6, 4224–4233, 2022.

[2] Narayanasamy, K., G. N. A. Mohammed, K. Savarimuthu, R. Sivasamy, and M. Kanagasabai, "A comprehensive analysis on the state-of-the-art developments in reflectarray, transmitarray, and transmit-reflectarray antennas," *International Journal of RF and Microwave Computer-Aided Engineering*, Vol. 30, No. 9, e22272, 2020.

[3] Abdelrahman, A. H., A. Z. Elsherbeni, and F. Yang, "Transmission phase limit of multilayer frequency-selective surfaces for transmitarray designs," *IEEE Transactions on Antennas and Propagation*, Vol. 62, No. 2, 690–697, 2014.

[4] Abdelrahman, A. H., A. Z. Elsherbeni, and F. Yang, "Transmitarray antenna design using cross-slot elements with no dielectric substrate," *IEEE Antennas and Wireless Propagation Letters*, Vol. 13, 177–180, 2014.

[5] An, W., S. Xu, F. Yang, and M. Li, "A double-layer transmitarray antenna using Malta crosses with vias," *IEEE Transactions on Antennas and Propagation*, Vol. 64, No. 3, 1120–1125, 2016.

[6] Pham, K. T., A. Clemente, E. Fourn, F. Diaby, L. Dussopt, and R. Sauleau, "Low-cost metal-only transmitarray antennas at Ka-band," *IEEE Antennas and Wireless Propagation Letters*, Vol. 18, No. 6, 1243–1247, 2019.

[7] Abdelrahman, A. H., A. Z. Elsherbeni, and F. Yang, "High-gain and broadband transmitarray antenna using triple-layer spiral dipole elements," *IEEE Antennas and Wireless Propagation Letters*, Vol. 13, 1288–1291, 2014.

[8] Yu, J., L. Chen, J. Yang, and X. Shi, "Design of a transmitarray using split diagonal cross elements with limited phase range," *IEEE Antennas and Wireless Propagation Letters*, Vol. 15, 1514–1517, 2016.

[9] Xu, H.-X., T. Cai, Y.-Q. Zhuang, Q. Peng, G.-M. Wang, and J.-G. Liang, "Dual-mode transmissive metasurface and its applications in multibeam transmitarray," *IEEE Transactions on Antennas and Propagation*, Vol. 65, No. 4, 1797–1806, 2017.

[10] Tian, C., Y.-C. Jiao, G. Zhao, and H. Wang, "A wideband transmitarray using triple-layer elements combined with cross slots and double square rings," *IEEE Antennas and Wireless Propagation Letters*, Vol. 16, 1561–1564, 2017.

[11] Dewi, M. F., A. Firdaus, S. Attamimi, M. Jusoh, M. Alaydrus, *et al.*, "Double-layer transmitarray antenna based on coupled rectangular loops at 9.8 GHz," *International Journal on Electrical Engineering and Informatics*, Vol. 14, No. 3, 499–513, 2022.

[12] Amriva, L., U. Umaisaroh, and M. Alaydrus, "A reflectarray antenna with inverted U patch backed by a metallic plate at 9.5 GHz," in *2020 IEEE International Conference on Communication, Networks and Satellite (Comnetsat)*, 102–105, Batam, Indonesia, Dec. 2020.

[13] Aryanian, I., A. Abdipour, and G. Moradi, "Design fabrication and test of an X-band dual polarized aperture-coupled reflectarray element for beam switching," *Turkish Journal of Electrical Engineering and Computer Sciences*, Vol. 25, No. 1, 539–551, 2017.

[14] Karimipour, M. and N. Komjani, "Bandwidth enhancement of electrically large shaped-beam reflectarray by modifying the shape and phase distribution of reflective surface," *AEU — International Journal of Electronics and Communications*, Vol. 70, No. 5, 530–538, 2016.

[15] Abadi, S. M. A. M. H., K. Ghaemi, and N. Behdad, "Ultra-wideband, true-time-delay reflectarray antennas using ground-plane-backed, miniaturized-element frequency selective surfaces," *IEEE Transactions on Antennas and Propagation*, Vol. 63, No. 2, 534–542, 2015.

[16] Magarotto, M., P. D. Carlo, L. Schenato, M. Santagiustina, A. Galtarossa, D. Pavarin, and A.-D. Capobianco, "Feasibility study on a plasma based reflective surface for SatCom systems," *Acta Astronautica*, Vol. 208, 55–61, 2023.

[17] Yang, S., Y. Chang, and B. Li, "A dual-band reflectarray antenna with low radar cross section," in *2023 International Applied Computational Electromagnetics Society Symposium (ACES-China)*, 1–3, Hangzhou, China, 2023.

[18] Muñoz-Rodero, T., P. Padilla, J. M. Fernández-González, J. L. Padilla, and J. F. Valenzuela-Valdés, "Broadband planar multilayered reflectarray based on circular stacked patches and reflective printed circuits for microwave communication systems," *Journal of Electromagnetic Waves and Applications*, Vol. 30, No. 17, 2344–2353, 2016.

[19] Florencio, R., R. R. Boix, J. A. Encinar, and G. Toso, "Optimized periodic MoM for the analysis and design of dual polarization multilayered reflectarray antennas made of dipoles," *IEEE Transactions on Antennas and Propagation*, Vol. 65, No. 7, 3623–3637, 2017.

[20] Qin, P.-Y., Y. J. Guo, and A. R. Weily, "Broadband reflectarray antenna using subwavelength elements based on double square meander-line rings," *IEEE Transactions on Antennas and Propagation*, Vol. 64, No. 1, 378–383, 2016.

[21] Gao, Q., J. Wang, Y. Li, and Z. Li, "A multiresonant element for bandwidth enhancement of circularly polarized reflectarray antennas," *IEEE Antennas and Wireless Propagation Letters*, Vol. 17, No. 5, 727–730, 2018.

[22] Guo, W.-L., G.-M. Wang, K.-Y. Liu, Y.-Q. Zhuang, and Q.-C. Ge, "Design of single-layered ultrawideband high-efficiency circularly polarized reflectarray," *IEEE Antennas and Wireless Propagation Letters*, Vol. 17, No. 8, 1386–1390, 2018.

[23] Zhang, L., S. Gao, Q. Luo, W. Li, Y. He, and Q. Li, "Single-layer wideband circularly polarized high-efficiency reflectarray for satellite communications," *IEEE Transactions on Antennas and Propagation*, Vol. 65, No. 9, 4529–4538, 2017.

[24] Han, C., Y. Zhang, and Q. Yang, "A novel single-layer unit structure for broadband reflectarray antenna," *IEEE Antennas and Wireless Propagation Letters*, Vol. 16, 681–684, 2016.

[25] Han, C., Y. Zhang, and Q. Yang, "A broadband reflectarray antenna using triple gapped rings with attached phase-delay lines," *IEEE Transactions on Antennas and Propagation*, Vol. 65, No. 5, 2713–2717, 2017.

[26] Xue, F., H.-J. Wang, M. Yi, G. Liu, and X.-C. Dong, "Design of a broadband single-layer linearly polarized reflectarray using four-arm spiral elements," *IEEE Antennas and Wireless Propagation Letters*, Vol. 16, 696–699, 2016.

[27] Aprilia, G. E., U. Umaisaroh, A. Firdausi, and M. Alaydrus, "Design of reflectarray comprising dipole structure at Ku-band," in *2021 International Symposium on Electronics and Smart Devices (ISESD)*, 1–4, Bandung, Indonesia, Jun. 2021.

[28] Fathurrahman, R., U. Umaisaroh, and M. Alaydrus, "Design of reflectarray antenna with ring-loaded patches for 5G applications," in *2021 International Conference on Radar, Antenna, Microwave, Electronics, and Telecommunications (ICRAMET)*, 60–63, Bandung, Indonesia, 2021.

[29] Ramadhani, A., A. Firdausi, U. Umaisaroh, and M. Alaydrus, "Design of cross and square slot with beamforming for microstrip reflectarray antenna at 28 GHz," in *2021 17th International Conference on Quality in Research (QIR): International Symposium on Electrical and Computer Engineering*, 182–186, Depok, Indonesia, Oct. 2021.

[30] Umaisaroh, U., A. Firdausi, F. Angesti, and M. Alaydrus, "Microstrip transmitarray antenna with three layered 5 x 5 crosslet and square slot patches at 38 GHz," in *2022 International Conference on Radar, Antenna, Microwave, Electronics, and Telecommunications (ICRAMET)*, 219–222, Bandung, Indonesia, Dec. 2022.

[31] Velly, T., A. Yonatan, U. Umaisaroh, and M. Alaydrus, "A reflectarray microstrip antenna with rectangular ring and cross patch at 28 GHz," in *2020 27th International Conference on Telecommunications (ICT)*, 1–4, Bali, Indonesia, Oct. 2020.

[32] Basar, E., M. D. Renzo, J. D. Rosny, M. Debbah, M.-S. Alouini, and R. Zhang, "Wireless communications through reconfigurable intelligent surfaces," *IEEE Access*, Vol. 7, 116 753–116 773, 2019.

[33] An, J., C. Xu, D. W. K. Ng, G. C. Alexandropoulos, C. Huang, C. Yuen, and L. Hanzo, "Stacked intelligent metasurfaces for efficient holographic MIMO communications in 6G," *IEEE Journal on Selected Areas in Communications*, Vol. 41, No. 8, 2380–2396, 2023.

[34] Abdulqader, A. J., J. R. Mohammed, and Y. A. Ali, "A T-shaped polyomino subarray design method for controlling side-lobe level," *Progress In Electromagnetics Research C*, Vol. 126, 243–251, 2022.

[35] Mohammed, J. R., "Beam-pattern control via thinned elements strategy in linear and planar phased arrays," *Progress In Electromagnetics Research Letters*, Vol. 111, 79–84, 2023.

[36] Younus, K. M. and J. R. Mohammed, "Array pattern reconfiguration using pixel method," *Applied Computational Electromagnetics Society Journal (ACES)*, Vol. 35, No. 3, 273–278, Mar. 2020.

[37] Subramaniam, D., M. Jusoh, T. Sabapathy, P. J. Soh, M. N. Osman, M. Alaydrus, C. J. Hodgkinson, S. K. Podilchak, and D. Schreurs, "High gain beam-steerable reconfigurable antenna using combined pixel and parasitic arrays," in *2020 50th European Microwave Conference (EuMC)*, 718–721, Utrecht, Netherlands, Jan. 2021.